Biomaterials 164 (2018) 11–21

Contents lists available at ScienceDirect

Biomaterials

journal homepage: www.elsevier.com/locate/biomaterials

Biodegradable near-infrared-photoresponsive shape memory implants based on black phosphorus nanofillers

Hanhan Xie [a, b, 1], Jundong Shao [a, 1], Yufei Ma [a, d, 1], Jiahong Wang [a], Hao Huang [a], Na Yang [a], Huaiyu Wang [a], Changshun Ruan [a, **], Yanfeng Luo [d], Qu-Quan Wang [b], Paul K. Chu [c], Xue-Feng Yu [a, *]

[a] Institute of Biomedicine and Biotechnology, Shenzhen Institutes of Advanced Technology, Chinese Academy of Sciences, Shenzhen 518055, PR China
[b] Department of Physics, Key Laboratory of Artificial Micro- and Nano-structures of Ministry of Education and School of Physics and Technology, Wuhan University, Wuhan 430072, China
[c] Department of Physics and Materials Science, City University of Hong Kong, Tat Chee Avenue, Kowloon, Hong Kong, PR China
[d] Research Center of Bioinspired Materials Science and Engineering, Key Laboratory of Biorheological Science and Technology, College of Bioengineering, Chongqing University, Chongqing 400030, PR China

ARTICLE INFO

Article history:
Received 4 September 2017
Received in revised form
14 February 2018
Accepted 19 February 2018
Available online 20 February 2018

Keywords:
Black phosphorus
Near-infrared light
Photothermal effect
Biodegradability
Two-dimensional materials

ABSTRACT

In this paper, we propose a new shape memory polymer (SMP) composite with excellent near-infrared (NIR)-photoresponsive shape memory performance and biodegradability. The composite is fabricated by using piperazine-based polyurethane (PU) as thermo-responsive SMP incorporated with black-phosphorus (BP) sheets as NIR photothermal nanofillers. Under 808 nm light irradiation, the incorporated BP sheets with concentration of only 0.08 wt% enable rapid temperature increase over the glass temperature of PU and trigger the shape change of the composite with shape recovery rate of ~100%. The *in vitro* and *in vivo* toxicity examinations demonstrate the good biocompatibility of the PU/BP composite, and it degrades naturally into non-toxic carbon dioxide and water from PU and non-toxic phosphate from BP. By implanting PU/BP columns into back subcutis and vagina of mice, they exhibit excellent shape memory activity to change their shape quickly under moderate 808 nm light irradiaiton. Such SMP composite enable the development of intelligent implantable devices, which can be easily controlled by the remote NIR light and degrade gradually after performing the designed functions in the body.

1. Introduction

In recent years, shape memory polymers (SMPs) are increasingly used in medical applications [1,2]. The advent of biocompatible (and in some cases even biodegradable) SMPs enables the development of novel implantable devices such as self-expanding stents, intelligent sutures, and active catheters as well as controlled drug release [3–9]. As intelligent materials, SMPs can recover from a temporary shape to a "remembered" permanent shape in response to a stimulus such as heat, light, or magnetic field [10–23]. Using light to trigger the shape recovery process is particularly appealing because light can more easily control remote activation with higher spatial and temporal resolution compared to other stimuli [17,22]. In general, photoresponsive SMPs are prepared by photo-cross-linking/isomerization with ultraviolet (UV) light or photothermal effects with near-infrared (NIR) light [15]. Obviously, only the latter strategy is suitable for *in vivo* biomedical applications because NIR light has excellent tissue penetration ability [24]. Therefore, there have been efforts to develop NIR-photoresponsive SMP composites by loading various photothermal nanofillers such as gold nanorods, carbon nanotubes, and graphene into thermo-responsive SMP matrix to absorb NIR light and convert the optical energy into heat [16,18,25–28]. However, these SMP composites generally suffers from the poor biodegradability of the nanofillers, which would stay in the body for a long period of time accentuating deleterious effects [29,30]. The development of SMP composites with both NIR-photoresponsive shape memory performance and biodegradability have tremendous clinical value, however it is still a great challenge now.

* Corresponding author.
** Corresponding author.
E-mail addresses: cs.ruan@siat.ac.cn (C. Ruan), xf.yu@siat.ac.cn (X.-F. Yu).
[1] These authors contributed equally to this work.

https://doi.org/10.1016/j.biomaterials.2018.02.040
0142-9612/

In this paper, we propose polyurethane/black-phosphorus (PU/BP) composite as a biodegradable SMP implant that permits remote control of its *in vivo* activities by NIR light. As a new class of 2D layered semiconductor, BP has received much attention due to the attractive physical properties [31–38] and immense potential in biomedicine [39–46]. BP sheets with different sizes are generally synthesized by liquid exfoliation [47–49] and exhibit large NIR extinction coefficient and high photothermal conversion ability [39,42]. Particularly, ultrasmall BP sheets (named BP quantum dots) have recently been well studied as the photothermal agent for cancer therapy [40,42]. Compared with other inorganic nanomaterials, BP is particularly attractive due to the inherent biocompatibility of P and natural decomposition in aqueous media producing nontoxic phosphate as the by-product [50,51].

Based on these considerations, here we synthesized BP sheets as the NIR photothermal nanofillers, and Piperazine-based PU, a new thermo-responsive SMP with controllable degradation [52,53], as the host polymer to incorporate the BP sheets. The PU/BP composite was fabricated and its NIR-photoresponsive shape memory effects were studied. Furthermore, systematic *in vitro* and *in vivo* experiments were performed to examine the biodegradability and biocompatibility of PU/BP implants, and their *in vivo* activities triggered by NIR light irradiation were also investigated.

2. Materials and methods

2.1. Materials

The BP crystals were purchased from a commercial supplier (Smart-Elements) and stored in an Ar glovebox in darkness. NMP (99.5%, anhydrous) was purchased from Aladdin Reagents. D,L-lactide, piperazine (PP), isosorbide (ISO), 1,6-hexamethylene diisocyanate (HDI), chloroform-d ($CDCl_3$), stannous octoate ($Sn(Oct)_2$), and dimethyl formamide were purchased from Sigma-Aldrich (California, USA). Ethanol, dichloromethane, chloroform, dimethylcarbinol, and methylbenzene were bought from Shanghai Lingfeng (Shanghai, China). PBS (pH = 7.4) was obtained from Gibco Life Technologies (AG, Switzerland) and Cy5.5 NIR fluorescence dye was obtained from Lumiprobe (US). All the chemicals were analytical reagent grade and used without further purification.

2.2. Synthesis of BP sheets

The BP sheets were prepared by a modified liquid exfoliation technique [49]. 25 mg of the BP crystals obtained were ground to BP powders and dispersed in 25 mL of NMP at an initial concentration of 1 mg/mL. The dispersion was sonicated in an ice bath for 10 h using a power of 300 W and then centrifuged for 10 min at 4000 rpm. The supernatant containing the BP sheets was centrifuged for another 10 min at 10,000 rpm. The precipitate was collected and re-suspended in the desired solution for further use.

2.3. Synthesis of PU

According to our previous reports [52], PU was synthesized by three steps. Firstly, poly (D, L-lactic acid) (PDLLA) diol were obtained by ring-opening polymerization of D,L-lactide in the presence of $Sn(Oct)_2$ as an initiator and PP as a co-initiator for 24 h at 150 °C under vacuum (PP/D,L-lactide = 1: 30 mol/mol, $Sn(Oct)_2$/D,L-lactide = 1: 5000 mol/mol). The PDLLA diol (PP-PDLLA) was purified three times by co-precipitation in chloroform/absolute ethyl alcohol system at room temperature and dried under vacuum at room temperature to a constant weight. The predetermined amounts of PP-PDLLA was terminated by HDI at 75 °C in a 250 mL three-necked flask under magnetic stirring with $Sn(Oct)_2$ as the catalyst and anhydrous toluene as the solvent. Finally, PP was added to the reaction system slowly for chain extension at 30 °C for 2 h. The mixture was purified by co-precipitation in toluene/ethanol and dried under vacuum at room temperature to a constant weight.

2.4. Preparation of PU/BP films

The PU/BP films were prepared by a solution casting method. The PU was dissolved with a BP chloroform solution under magnetic stirring at room temperature with different BP quantities between 0 and 0.16 wt%. The dispersion was poured into a polytetrafluoroethylene (PTFE) mold to form a uniform film. The solvents were allowed to evaporate for 48 h until the films were formed and dried under vacuum to a constant weight.

2.5. Preparation of PU/BP column

The PU/BP column was prepared by a thermoplastic method. The PU/BP composite was introduced into a self-made tubular PTFE mold, and then heated at 140 °C for 2 h to melt the molding. After cooling to room temperature, the PU/BP column was fabricated.

2.6. Characterization

The scanning electron microscopy (SEM) images were obtained on the field-emission SEM (NOVA NANOSEM430, FEI, Netherlands) at 5–10 kV. High-resolution transmission electron microscopy (HR-TEM) was performed on the Tecnai G2 F20 S-Twin transmission electron microscope at an acceleration voltage of 200 kV. Atomic force microscopy (AFM) was conducted on the drop-cast flakes on Si/SiO2 substrates on the MFP-3D-S atomic force microscope (Asylum Research, USA) using the AC mode (tapping mode) in air. X-ray photoelectron spectroscopy (XPS) was carried out using the Thermo Fisher ESCALAB 250Xi XPS. The Raman scattering spectra were obtained on a Horiba Jobin-Yvon LabRam HR-VIS high-resolution confocal Raman microscope equipped with a 633 nm laser as the excitation source. The absorption spectra were acquired on a Lambda25 spectrophotometer (PerkinElmer) with QS-grade quartz cuvettes under room temperature. The BP concentration was determined by inductively-coupled plasma optical emission spectrometry (ICP-OES) (7000DV, PerkinElmer). Fourier transform infrared spectroscopy (FTIR) was carried on a BRUKER VERTEX 70. The nuclear magnetic resonance (NMR) spectra were acquired on an AVANCE III 400 spectrometer with $CDCl_3$ as the solvent. The glass temperature (T_g) of PU was measured according to Differential scanning calorimetry (DSC) analyses on the TA Instrument Q20 on an aluminum pan at a heating rate of 10 °C min^{-1} under a nitrogen flow of 50 mL min^{-1}. The molecular weight and dispersity of PU were obtained by gel permeation chromatography (GPC) with multi-angle laser light scattering (Malvern Viscotek 270max). The shape memory images were captured by a digital single-lens reflex camera (Nikon, D5200, Thailand).

2.7. Photothermal experiments

A fiber-coupled continuous semiconductor diode laser (808 nm, KS-810F-8000, Kai Site Electronic Technology Co., Ltd. Shaanxi, China) was employed as the light source. To study the photothermal effects of the BP sheets, a 1 cm path length quartz cuvette containing 0.5 mL of the sample was irradiated with the laser at a power density of 1.6 W/cm^2 for 5 min. The laser spot was adjusted to fully cover the entire surface of the sample. To determine the photothermal effects of PU/BP composite film, the film was cut into approximate dimensions of 9 × 6 × 1 mm and irradiated with the

laser at a power density of 0.17 W/cm^2 for 50 s. An infrared thermal imaging camera (Fluke TiS75, USA) was used to monitor the temperature change.

2.8. Shape memory experiments

To measure the photothermal induced shape memory properties of PU/BP film, the film with dimensions of 9 × 6 × 1 mm was folded in half at 60 °C and placed at 4 °C for shape fixation. After fixing the temporary shape, the film was brought back to room temperature for laser exposure. The thermal response time was recorded until a complete shape change of the film was achieved. The shape memory behavior was monitored by a digital single-lens reflex camera and the shape recovery rate was calculated by measuring the variation of the angle between the two halves of the film. The measurements were repeated three times.

2.9. In vitro cytotoxicity assays

The human mesenchymal stem cells (hMSCs) and mouse fibroblast (L929) cells were purchased from the American Type Culture Collection (ATCC). These cells were cultured in the H-DMEM medium supplemented with 10% (v/v) fetal bovine serum (FBS) and maintained in a humidified atmosphere of 37 °C with 5% CO_2. The PU/BP films with different BP quantities from 0.00 to 0.16 wt% were divided into two groups, with irradiation and without irradiation. The films were disinfected by immersion in 75% (v/v) ethanol for 30 min and washed twice with PBS. Each film (with approximate dimensions of 9 × 6 × 1 mm) on the well of a 24-well plate was seeded with 1×10^4 cells in 20 μL of the cell culture medium for 2 h and then 1 mL of the cell culture medium was added. The cell viability was determined by the CCK-8 assay. A microplate spectrophotometer (Varioskan Flash 4.00.53, Finland) was employed to measure the optical absorbance at 450 nm as an indicator of viable cells. The cell viability was calculate by the following formula: cell viability (%) = (mean of Abs. value of treatment group/mean Abs. value of control) × 100%.

2.10. In vitro degradation

The *in vitro* degradation of the samples (approximate dimensions of 9 × 6 × 1 mm) was performed in the closed sample vials containing ultrapure water or PBS solution (0.1 M, pH 7.4) as the degradation medium. The samples were divided into three groups: (a) PU; (b) PU/BP; (c) PU/BP after irradiation. The degree of degradation was evaluated by determining the pH, phosphate concentration, residual weight, and water absorption. All the experiments were performed in a horizontal shaking incubator at 37 °C. To measure the pH of the degradation medium, 4 mL of ultrapure water were added to the vials and measured once a week in a period of 12 weeks using a pHS-25 pH meter (Shanghai precision & scientific instrument, China). Each group containing three samples was prepared and the final pH was the average of three samples. The change in the phosphate concentration of the degrading PU/BP samples was measured by a colorimetric method (Quanti-Chrom DIPI500, BioAssay Systems) [54]. The residual weight and water absorption rate were examined according to a reported method [53]. Each group containing 36 samples was added to 36 vials, respectively, and each vial contained 4 mL of PBS. Three vials of the sample were taken, washed with ultrapure water, and dried under vacuum to a constant weight at the end of each week during a period of 12 weeks. The residual weight and water absorption rate of the samples were calculated by the following formulas: residual weight (%) = $W_r \times 100/W_o$, where W_o and W_r were weights of the samples before and after degradation, respectively, and water absorption (%) = $W_t \times 100/W_o$, where W_o and W_t were the weights of the degrading samples before and after vacuum drying, respectively.

2.11. In vivo toxicity examination

Twenty healthy female Balb/c mice (6 weeks old) were purchased from Slac Laboratory Animal Co., Ltd. (Hunan, China) and all the *in vivo* experiments followed the protocols approved by the Animal Care and Use Committee of the Shenzhen Institutes of Advanced Technology, Chinese Academy of Sciences. The mice were randomly divided into 4 groups: (a) Control; (b) PU; (c) PU/BP; (d) PU/BP after irradiation. In the *in vivo* toxicity study, a skin incision was made at the back subcutis of each mouse followed by the sample implantation. Afterwards, each mouse was monitored during the 2 month after the sample was implanted and compared with the control mice. After the mice were sacrificed, complete blood panel analysis and serum biochemistry assay were carried out at the Shanghai Research Center for Biomodel Organism by collecting 0.8 mL blood from the mice. The major organs (heart, liver, spleen, lung and kidney) were harvested, fixed in 10% neutral buffered formalin, processed routinely into paraffin, sectioned at 8 mm, stained with haematoxylin and eosin, and examined by digital microscopy.

2.12. In vivo shape memory behavior

Twenty healthy female Balb/c nude mice (6 weeks old) were purchased from Slac Laboratory Animal Co., Ltd. (Hunan, China). The fluorescent labeled PU/BP column was prepared by adding 2 mg Cy5.5 into the PU/BP composite by using a thermoplastic method mentioned above. And then the PU/BP column were stretched to the diameter of approximately 1 mm at 60 °C, placed at 4 °C for shape fixation, and brought back to room temperature for laser exposure (808 nm, 0.17 W/cm^2). The shape memory behavior was monitored by a digital single-lens reflex camera. In the *in vivo* biomedical evaluation, the fluorescent labeled PU/BP column with a diameter of approximately 1 mm and length of approximately 10 mm was implanted into the back subcutis of the female Balb/c nude mouse and exposed to the 808 nm laser (0.17 W/cm^2) for 0, 30 and 60 s, respectively. The fluorescent labeled PU/BP column with a diameter of approximately 0.5 mm and length of approximately 8 mm was implanted into the vagina of the mouse and exposed to the 808 nm laser (0.5 W/cm^2) for 0, 30 and 60 s, respectively. The shape memory behavior of the PU/BP column in the back subcutis or vagina of the mouse were monitored by a fluorescence (Xenogen IVIS-Spectrum) imaging system. A peak wavelength of 675 nm was chosen as the excitation source and the Cy5.5 bandpass emission filter (680–720 nm) was conducted for 200 ms exposure time for each image frame.

3. Results and discussion

3.1. Synthesis and characterization of BP sheets

The BP sheets were synthesized by using a modified liquid exfoliation technique and characterized by SEM, HR-TEM, XPS, Raman spectroscopy, and AFM. As shown in Fig. 1a–h, the BP sheets have a 2D sheet-like morphology with an average lateral size of about 375 ± 95 nm and thickness of about 40 ± 16 nm. The HR-TEM image discloses lattice fringes of 0.22 nm ascribed to the (002) plane of the BP crystal [55]. The chemical composition of BP sheets was determined by XPS after sputtering for 5 min to get rid of surface contamination (see Fig. 1d and Fig. S1). In the XPS spectra, the $2p_{3/2}$ and $2p_{1/2}$ peaks at 129.5 and 130.3 eV, respectively, are

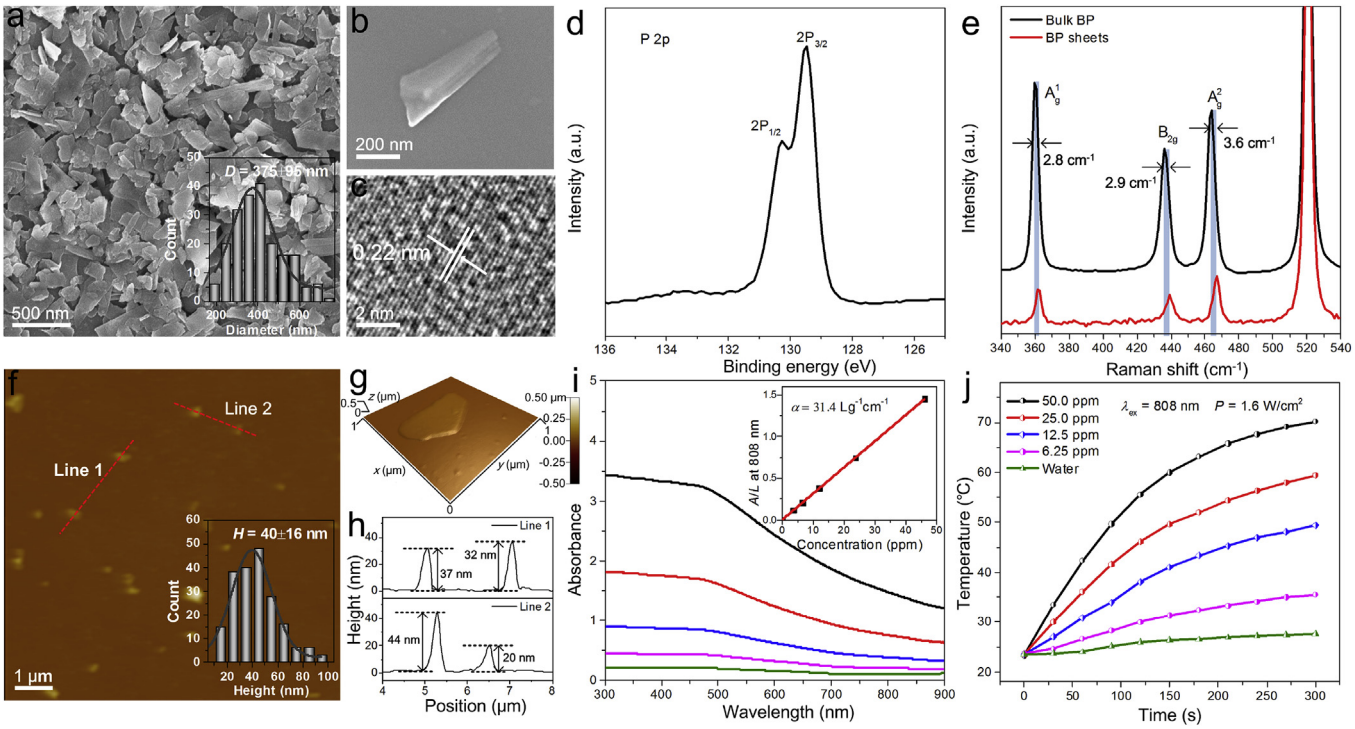

Fig. 1. Characterization of BP sheets: (a) SEM image with the inset statistical analysis of the size of 200 BP sheets; (b) Magnified SEM image; (c) HR-TEM image; (d) XPS spectrum; (e) Raman scattering spectra; (f) AFM image with the inset statistical analysis of the thickness of 200 BP sheets; (g) 3D AFM image of one sheet; (h) Typical height profiles along the red lines in f; (i) Absorption spectra of the BP sheets dispersed in water with different concentrations (0, 3.5, 6.7, 12.0, 23.7 and 46.1 ppm). Inset: normalized absorbance intensity over characteristic length of the cell (A/L) at different concentrations for $\lambda = 808$ nm; (j) Photothermal heating curves of the BP sheets dispersed in water with different concentrations irradiate by an 808 nm laser (1.6 W/cm^2). (For interpretation of the references to color in this figure legend, the reader is referred to the Web version of this article.)

characteristic of crystalline BP [35]. In the Raman spectra of the BP sheets, the three prominent peaks can be attributed to one out-of-plane phonon mode (A^1_g) at 362.5 cm^{-1} and two in-plane modes, B_{2g} and A^2_g, at 438.9 and 467.2 cm^{-1}, respectively. The A^1_g, B_{2g}, and A^2_g modes of BP sheets red-shift by about 2.8, 2.9, and 3.6 cm^{-1}, respectively, compared to bulk BP. These results demonstrate successful synthesis of the BP sheets.

The optical properties of the BP sheets dispersed in an aqueous solution were examined. As shown in Fig. 1i, the BP sheets show a broad absorption band spanning the UV and NIR regions similar to other 2D layered materials [56,57]. The absorbance intensity per cell length (A/L) is determined from the absorbance spectra at 808 nm. The BP concentration (C) is determined by ICP-OES. Using Beer's law ($(A/L = \alpha C)$, the BP's extinction coefficient α is calculated to be 31.4 Lg^{-1}cm^{-1} from the slope of the A/L versus concentration (C) plot (inset in Fig. 1i). It is larger than those of most reported photothermal nanomaterials such as Au nanorods, GO sheets, WS_2 sheets, and BP quantum dots [58–60].

To evaluate the NIR photothermal performance, different concentrations of BP sheets were dispersed in aqueous solutions and exposed to an NIR laser (808 nm, 1.6 W/cm^2). The solution temperature as a function of time is monitored (see Fig. 1j). At a very low concentration (50 ppm), the solution temperature increases by 47.0 °C after irradiation for only 5 min. In contrast, the temperature of water increases by only 4.1 °C, indicating that the BP sheets can efficiently convert NIR light into thermal energy.

3.2. Preparation and characterization of PU and PU/BP composite

The shape memory PU is one of the most interesting SMPs due to its shape memory characteristics and tailorable performance boding well for biomedical applications. In general, PU consists of two segments: a hard segment determining the permanent shape and soft one fixing the temporary shape below the transition temperature. Here, typical biodegradable thermo-responsive PU was synthesized with PDLLA diol as the soft segment and hexamethylene diisocyanate and piperazine as the hard segment. The hard-soft phase separation and thermo-responsive shape memory behavior of PU are presented in Fig. S2. The chemical structure was determined by FTIR (Fig. S3a) and NMR (Fig. S3b). DSC (Fig. S3c) and GPC (Fig. S3d) show that the PU has a T_g of 49.5 °C and molecular weight (M_w) of 84,457 Da. This polymer is suitable for medical implants for the desirable shape memory, mechanical, and natural degradation properties, which can further be tailored by altering the contents of piperazine in PU [53].

The PU/BP composite films were prepared by a solution casting method (see Fig. 2a) in which the piperazine-PU as the host polymer embedded with the BP sheets. Typically, the PU was dissolved with a BP chloroform solution, and the dispersion was poured into a PTFE mold to form a uniform film. The solvents were allowed to evaporate until the films were formed and dried under vacuum to a constant weight. Fig. 2b show the films of the PU/BP composites with different BP concentrations from 0 to 0.16 wt%. These PU/BP films have smooth surface and the color darkens gradually with the increased BP concentration. A random and homogeneous dispersion of BP in PU can be obtained without clusters or agglomerates due to the good dispersion of the BP sheets. As shown in Fig. S4, the three prominent peaks at 362.5, 439.5, and 467.1 cm^{-1} are associated with A^1_g, B_{2g}, and A^2_g of BP, respectively, confirming successful incorporation of BP sheets in the film. The hydrophilicity-hydrophobicity was further evaluated by measuring the water contact angles. As shown in Fig. S5, the PU/BP film ($103.0 \pm 1.2°$) shows similar hydrophobicity as pure PU ($101.5 \pm 2.1°$) and so the embedded BP does not affect the PU surface energy.

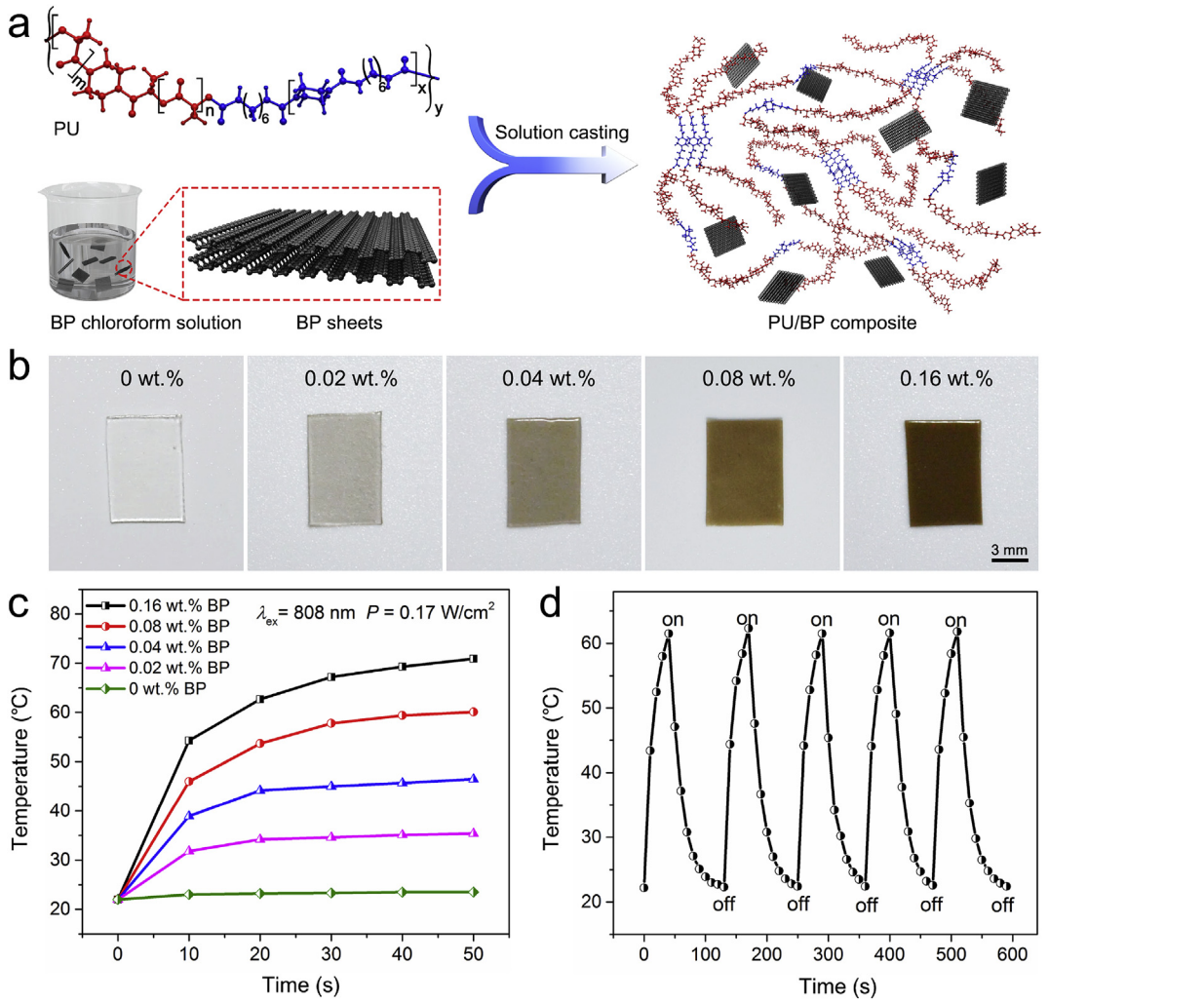

Fig. 2. (a) Preparation procedures of PU/BP composite; (b) Photographs of the PU/BP films with different BP concentrations; (c) Photothermal heating curves of the PU/BP films with different BP concentrations irradiated by the 808 nm laser (0.17 W/cm^2); (d) Temperature elevation of the PU/BP film with 0.08 wt% BP for five laser on/off cycles.

The NIR photothermal performance of the PU/BP films with different BP concentrations was assessed. The films were irradiated by an 808 nm laser (0.17 W/cm^2) and their temperature as a function of time was monitored. As shown in Fig. 2c, an obvious increase in the temperature can be observed as the BP concentration is increased. The film with 0.08 wt% of BP shows a temperature increase from 22.0 to 60.1 °C (over T_g of PU) after laser irradiation with a low power intensity of only 0.17 W/cm^2 for 50 s. In contrast, the temperature of the pure PU film increases by only 1.5 °C after such irradiation. Moreover, compared to the laser power intensity used to obtain photothermal effects from BP sheets in an aqueous solution (1.6 W/cm^2), the PU/BP film shows more pronounced photothermal effects at a much lower laser power (0.17 W/cm^2). This is probably ascribed to the fact that the opaque PU/BP film is more efficient than the BP sheets solution for light absorption. To further assess the photothermal stability of the PU/BP composite film, the time-dependent temperature of the film with 0.08 wt% BP upon radiation with the NIR laser for 50 s (Laser on) was determined, followed by natural cooling to room temperature after the NIR laser was turned off (Laser off). As shown in Fig. 2d, even when the cycle has been repeated 5 times, the photothermal efficiency does not decline, which exhibit the good photostability of the composite. These results demonstrate the excellent photothermal performance of the PU/BP film, in which only 0.08 wt% BP incorporation enable the rapid temperature increase over the T_g of PU.

3.3. NIR-photoresponsive shape memory performance

The shape memory performance of the PU/BP composite under NIR light irradiation was investigated. The PU/BP films heated to 60 °C (over T_g) were folded in half and cooled to 4 °C for fixation. After fixation of the temporary shape, the film was brought back to room temperature (25 °C, below T_g) for light irradiation with an 808 nm laser (0.17 W/cm^2). As shown in Fig. 3a, the PU/BP film under NIR irradiation can gradually recover its initial unrolled shape. To estimate its shape recovery rate, the variation in the angle between the two halves of the film during irradiation was measured (see Fig. 3b). After irradiation for 50 s, the deformed PU/BP film can be recovered 100% of the original shape and it is more efficient than many SMPs such as hydrogels (98%), poly(ε-caprolactone) (94%), and polyetherurethane (80%) [14,61,62]. The good NIR-photoresponsive shape memory performance stems from the excellent NIR photothermal performance of BP sheets together with the excellent thermo-responsivity of PU SMP.

The NIR light triggered shape memory behavior of the PU/BP composite was further investigated with a film rolled into a scroll as

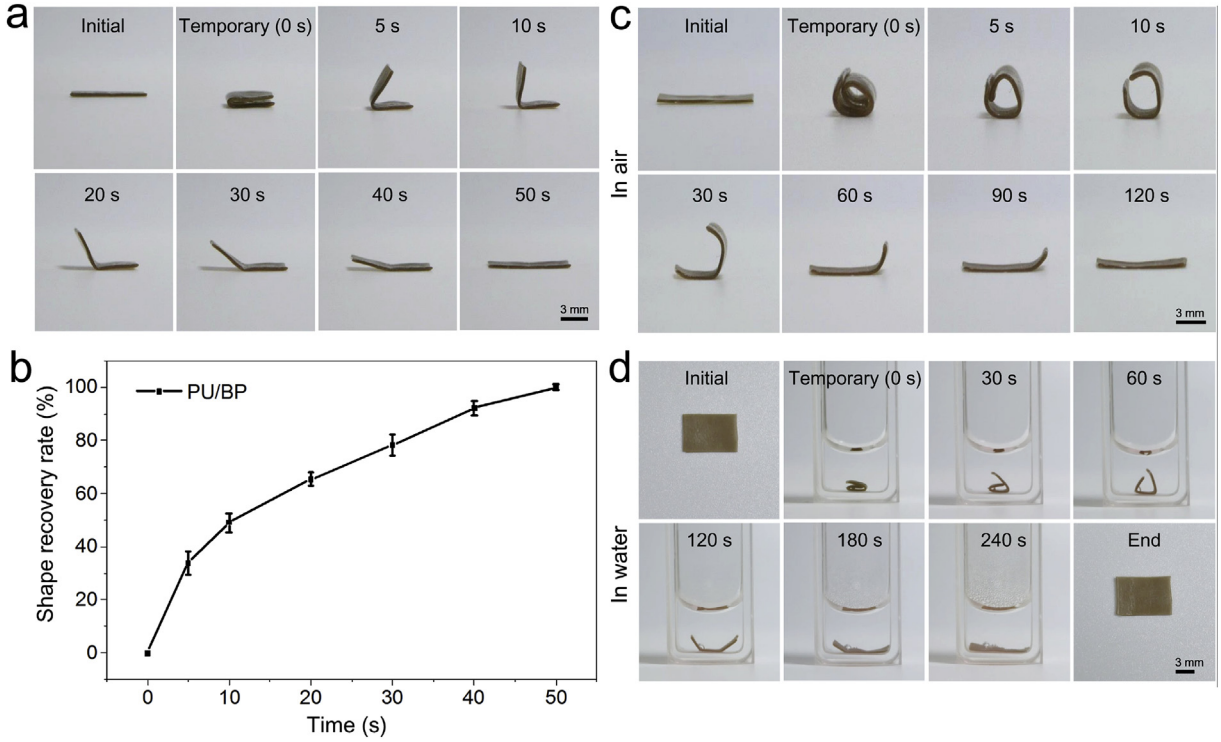

Fig. 3. (a) Photographs showing the NIR light triggered shape memory behavior of a folded PU/BP film; (b) Plot of the shape recovery rate vs irradiation time; (c, d) Photographs showing the NIR light triggered shape memory behavior of a rolled PU/BP film put in (c) air and (d) water.

the temporary shape. Fig. 3c show that the film placed in air can recover the initial unrolled shape after irradiation for 120 s (808 nm, 0.17 W/cm^2). Even if the film was immersed into a water solution, complete recovery could be observed after exposure to a laser with the power intensity of 1.6 W/cm^2 for 240 s (see Fig. 3d). The longer recovery time and higher laser power intensity are mainly due to the faster heat dissipation in water than air. It suggests the good activity of PU/BP composite in physiological environments.

3.4. *In vitro* cytotoxicity

The *in vitro* cytotoxicity of the PU/BP composite was evaluated by co-culturing with hMSCs and L929 cells, which were widely used in cytotoxicity evaluation [63]. As shown in Fig. 4a and b, the cells seeded on the PU/BP films with different BP concentrations from 0 to 0.16 wt% are more than 90% viable after 24 h, suggesting that both pure PU and PU/BP have low cytotoxicity to both hMSCs and L929 cells. Moreover, there is no signficant difference in the cell viability bettween the PU/BP films before and after laser irradiation at a power density of 0.17 W/cm^2 for 50 s. It demonstrates that the laser irradiation would not induce the additional cytotoxicity of the PU/BP composite.

3.5. Degradation behavior

The degradation behavior of the PU/BP composite was investigated by using an *in vitro* degradation model described previously [53]. The pH, phosphate concentration, residual weight, and water absorption were monitored at predetermined time intervals with pure PU as the control. Fig. 4c shows the solution pH variation during degradation. For the pure PU film, the pH declines sharply due to breakage of ester/urethane/urea bonds and release of acidic groups as observed previously [53]. With regard to the PU/BP film, the pH declines more quickly because the degradation of BP releases phosphate, which reduces the pH and increase the phosphate concentration (see Fig. 4d).

The residual weight of the films during degradation is shown in Fig. 4e. The small change reveals slight degradation during the first five weeks caused by swelling and hydration. Afterwards, the sharp decrease of the residual weight indicates that the fragments in PU are cleaved and dissolve in the aqueous medium. For the PU/BP film, the degradation of PU triggers the release of embedded BP which is converted quickly to phosphate to decrease the pH, thus accelerate the film degradation. When the degradation time is increased to 12 weeks, the residual weight of the PU/BP film decreases to 29.35 ± 1.59% of the original value compared to a decrease of 39.24 ± 2.29% of the pure PU film. It indicates that the PU/BP film has a smaller residual weight after the second stage of the degradation. Fig. 4f further shows the variation of the water absorption during the degradation process. For pure PU film, the water absorption stems from the surface micropores that can trap water [64]. With regard to the PU/BP film, the BP degradation leads to the formation of more micropores and thus induces more water absorption, which creates more hydration sites and accelerates the film degradation.

The above degradation investigations demonstrate that the incorporated BP sheets can accelerate the degradation of PU, and their degradation product is phosphate. Considering PU is well known a biodegradable polymer with degradation products are non-toxic carbon dioxide and water, the PU/BP composite possesses excellent biodegradability with non-toxic by-products. In addition, there is no signficant difference in all the degradation parameters of the PU/BP composite film with and without the NIR light irradiation (0.17 W/cm^2, 50 s), indicating that laser exposure does not affect degradation of the PU/BP composite.

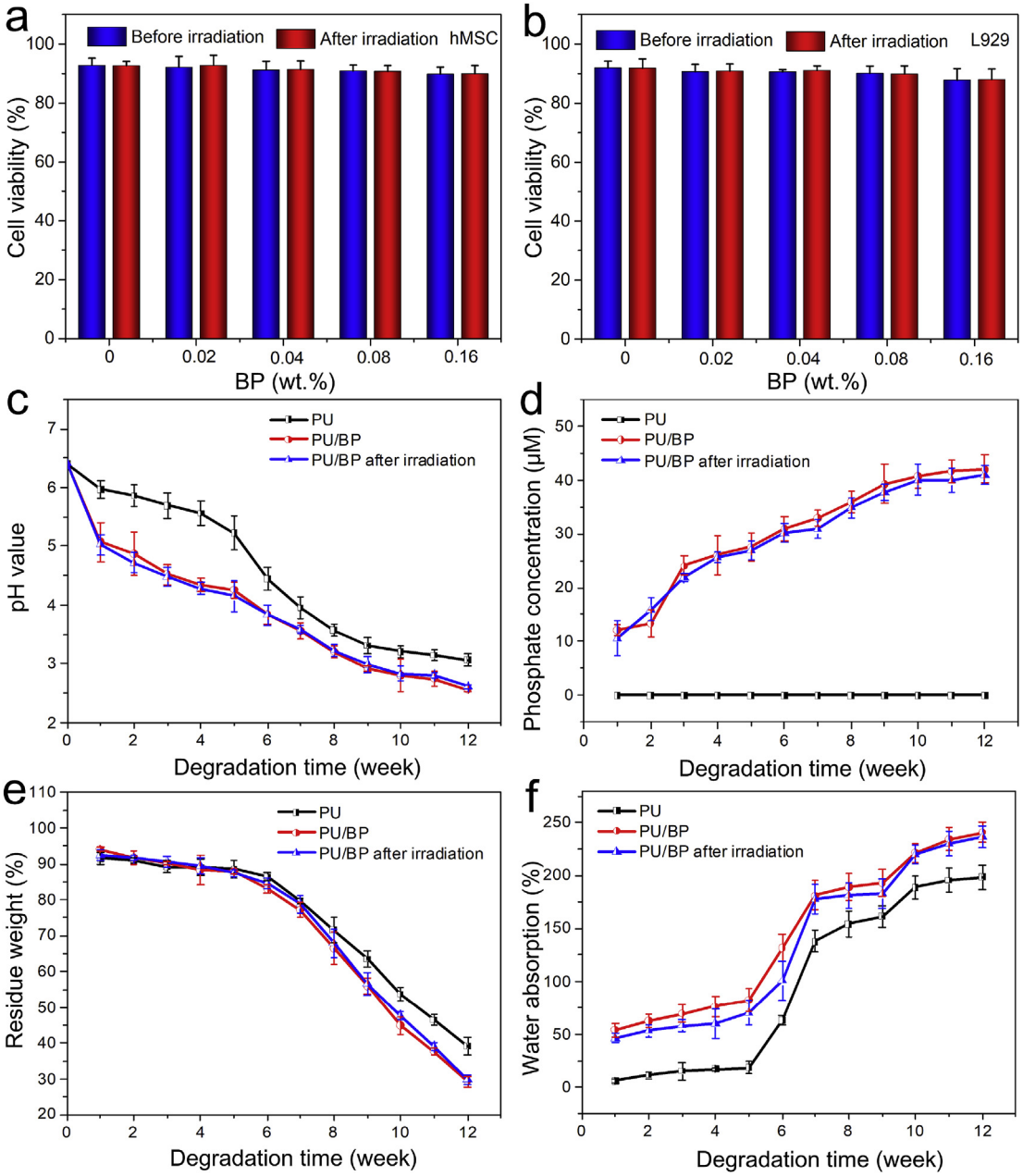

Fig. 4. (a, b) Cytotoxicity of the PU/BP films with different BP concentrations incubated with (a) hMSCs and (b) L929 cells for 24 h; (c) pH; (d) Phosphate concentration; (e) Residual weight; (f) Water absorption as a function of time during degradation of PU, PU/BP, and PU/BP under NIR irradiation (0.17 W/cm^2, 50 s).

3.6. *In vivo toxicity*

The potential *in vivo* toxicology of the PU/BP composite was evaluated systematically. Twenty healthy female Balb/c mice were randomly divided into 4 groups and treated to variable conditions, including: (1) control group without any treatment, (2) PU implanted into the mice, (3) PU/BP implanted into the mice, (4) PU/BP after irradiation implanted into the mice. Each mouse was monitored during the 2 months after the samples were implanted and compared with the control mice. The *in vivo* toxicology was determined by haematological, biochemical, and histological analyses. The white blood cells (WBC), red blood cells (RBC), mean corpuscular volume (MCV), platelets (PLT), mean corpuscular haemoglobin (MCH), haemoglobin (HGB), haematocrit (HCT), and mean corpuscular haemoglobin concentration (MCHC) were measured (Fig. 5a). Compared with the control group, almost all the parameters obtained from the PU and PU/BP groups are normal and no meaningful difference can be found. It demonstrates that the PU/BP composite do not produce deleterious effects. Blood biochemical examination was also carried out and the biochemical parameters including alanine transaminase (ALT), aspartate transaminase (AST), total protein (TP), blood urea nitrogen (BUN), albumin (ALB), alkaline phosphatase (ALP), direct bilirubin (DBIL), and glucose (GLU) were examined (Fig. 5b). Again no significant toxic side effects can be observed from the PU and PU/BP groups. Since the ALT, AST and ALP levels are usually associated with the functions of the liver and kidney of mice [65], the results confirm that the PU/BP implant does not cause obvious hepatic and kidney toxicity.

In addition, the corresponding histological changes in the

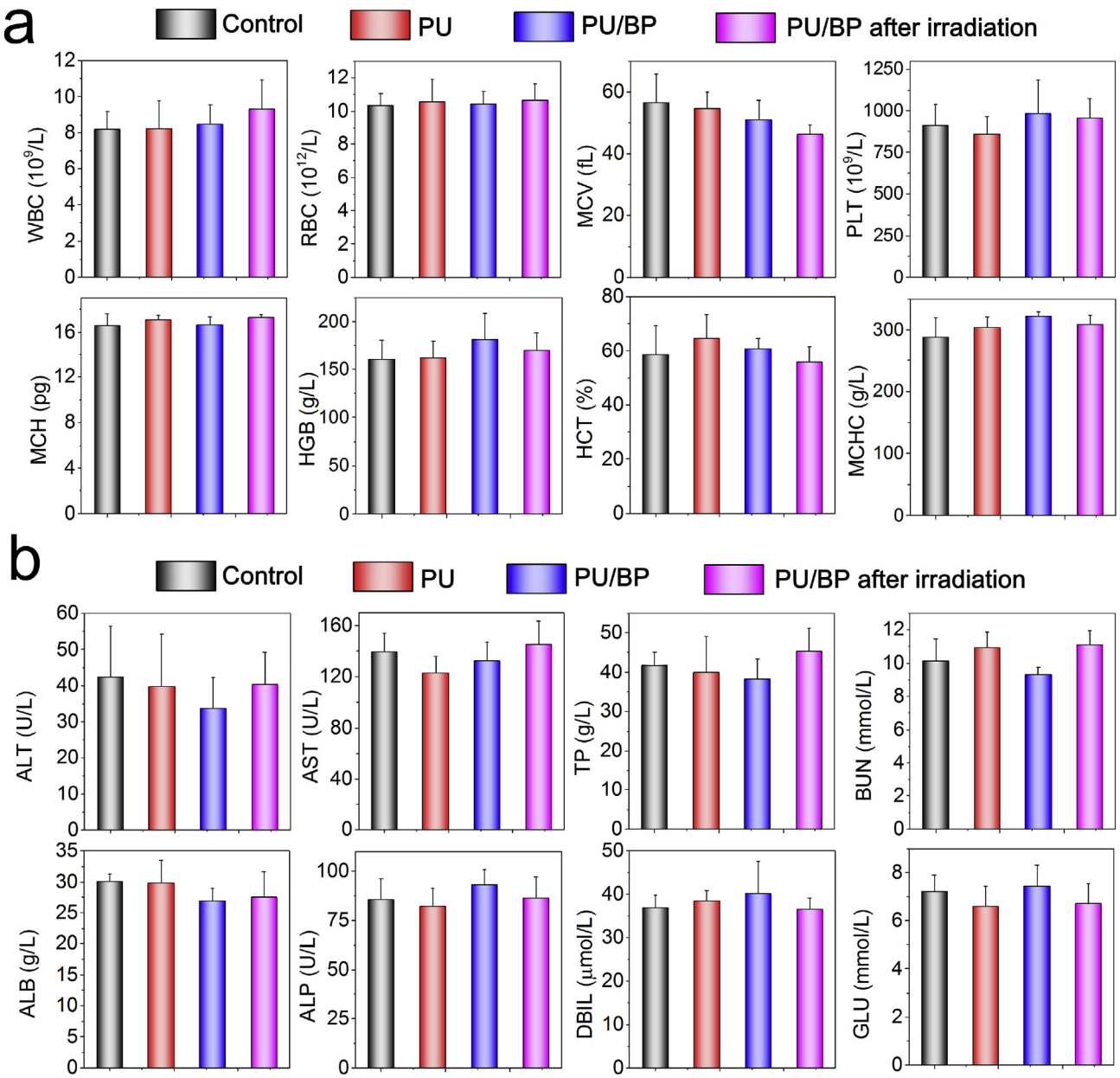

Fig. 5. (a) Hematology analysis of the mice after PU/BP composite implantation. The data were collected after two months. The following parameters were measured: WBC, RBC, MCV, PLT, MCH, HGB, HCT and MCHC. (b) Blood biochemistry data of the mice with PU/BP composite two months after implantation with parameters including ALT, AST, TP, BUN, ALB, ALP, DBIL, and GLU.

organs were examined by immunohistochemistry. The major organs including the heart, liver, spleen, lung, and kidney are collected and sliced for haematoxylin and eosin (H&E) staining and histological examination. No appreciable abnormality is observed from the major organs in comparison with the control group (see Fig. 6). In general, there are no evident histopathological abnormalities or lesions in the treated groups suggesting good biocompatibility of the PU/BP composite.

3.7. *In vivo shape memory behavior*

Due to its excellent shape memory performance and biodegradability as well as biocompatibility, the potential of the PU/BP composite for biomedical applications is further assessed. It is well known that contraception can be achieved by using a column to internal mechanical occlusion of the fallopian tubes [66]. The PU/BP composite was then made into a column by a thermoplastic method and their shape memory process under NIR laser irradiation was schematically described shown in Fig. 7a. Briefly, the PU/BP composite was introduced into a self-made tubular PTFE mold, and then heated at 140 °C for 2 h to melt the molding. After cooling to room temperature, the PU/BP column was fabricated and subsequently stretched to the appropriate size. Then the stretched column was placed at 4 °C for shape fixation and brought back to room temperature for laser exposure. Under NIR light irradiation, the stretched column can effectively recover its initial shape, and these appealing shape memory properties can be further used for fallopian tubes contraception. In order to provide a more visual description about how using this column for fallopian contraception. Fig. 7b gives the schematic illustration of the fallopian tubes

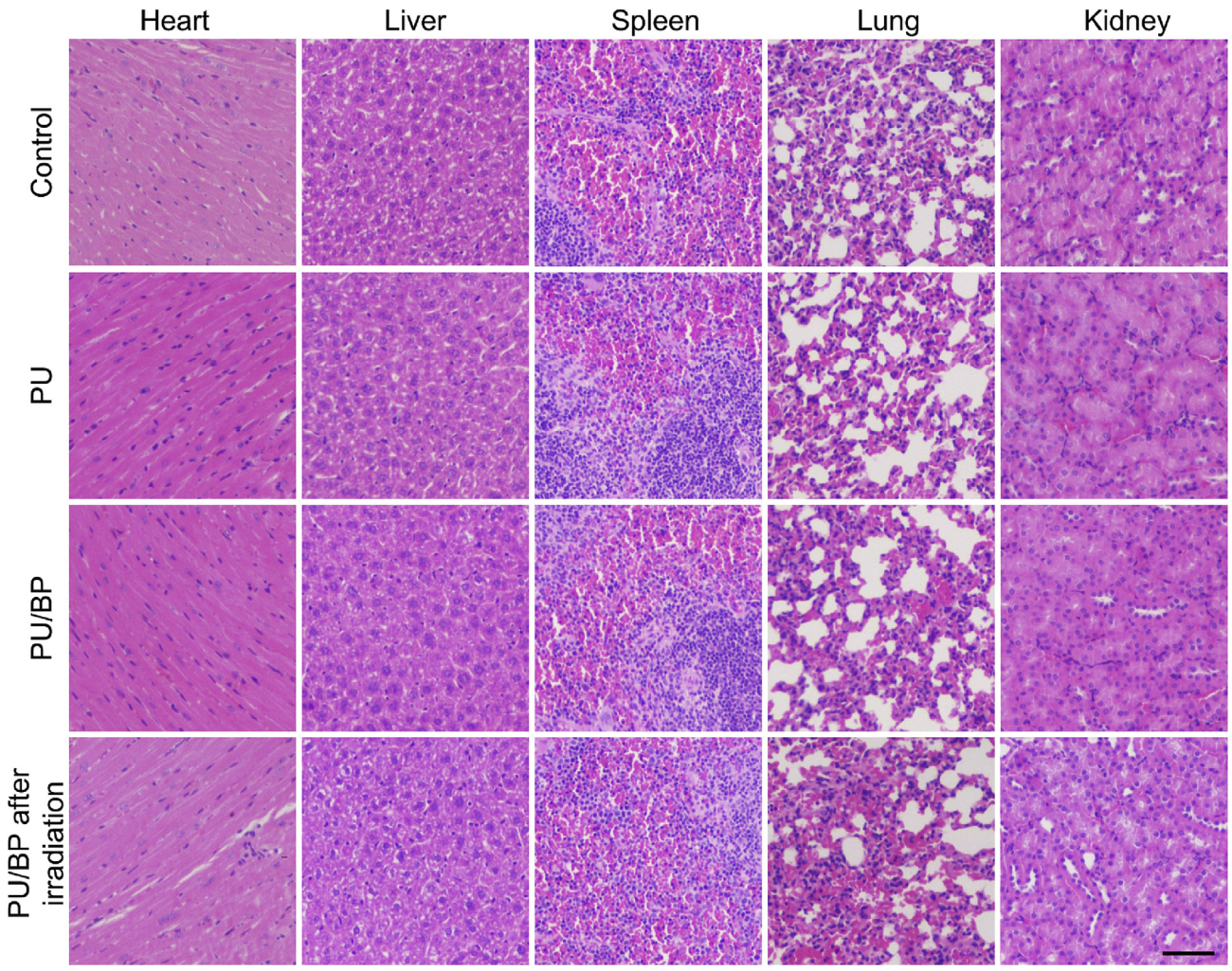

Fig. 6. Histological data acquired from the heart, liver, spleen, lung, and kidney two months after implantation of the PU/BP composite (scale bars = 100 mm).

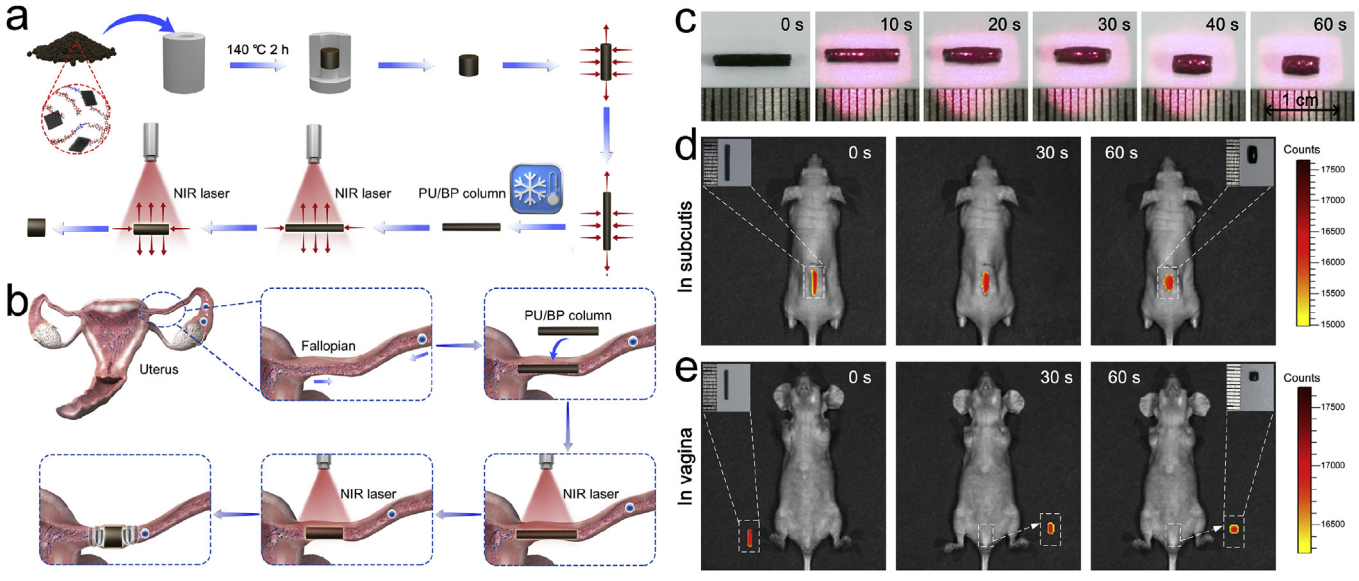

Fig. 7. (a) Schematic illustration of the fabrication of the PU/BP column and their shape memory process under NIR laser irradiation. (b) Schematic illustration of the fallopian tubes contraception. (c) Photographs showing NIR-photoresponsive shape recovery behavior of a fluorescent PU/BP column. The fluorescence images and photographs show the *in vivo* shape recovery behavior of the PU/BP columns in (d) subcutis of the mouse under an 808 nm NIR light (0.17 W/cm^2) irradiation and (e) vagina of the mouse under an 808 nm NIR light (0.5 W/cm^2) irradiation.

contraception by using this column. The stretched column was implanted into the proximal of the fallopian tube, and then gradually recovered to its initial shape remotely controlled by using the NIR laser. The recovered column was large enough to occlude the fallopian tube and prevent the integration of sperms and eggs for the purpose of contraception. In order to facilitate observation, Cy5.5, a commonly used fluorescent dye, was utilized to label the PU/BP column (see Fig. S6) by entrapping it into the composite using a thermoplastic method mentioned above. Shape memory behaviors of the PU/BP column *in vivo* were monitored by a fluorescence (Xenogen IVIS-Spectrum) imaging system. As shown in Fig. 7c, upon irradiation with an 808 nm laser (0.17 W/cm^2) for 60 s, the stretched fluorescent PU/BP column becomes thicker and shorter quickly, demonstrating the good NIR-photoresponsive shape memory performance of the PU/BP column.

In order to explore the feasibility of fallopian tubes contraception, the fluorescent PU/BP column was further implanted in the back subcutis of a female Balb/c nude mouse to study its *in vivo* activity (see Fig. 7d). When the column was irradiated with an 808 nm laser with power intensity of only 0.17 W/cm^2 for 60 s, its diameter changes from 1 to 2.8 mm and length changes from 10 to 4.8 mm, demonstrating its efficient shape recovery property *in vivo*. Furthermore, another fluorescent PU/BP column was implanted into the vagina of a mouse to simulate a fallopian tube (see Fig. 7e). Since the vagina is as deep as ~5 mm, Cy5.5 fluorescence cannot penetrate the tissue and hence, the column is taken out for fluorescence imaging. Even so, the shape memory behavior of the PU/BP column can be triggered by the 808 nm light, which has better tissue penetration ability than visible light. The laser power intensity is 0.5 W/cm^2, which is still much lower than that generally used in previously reported photothermal cancer therapy applications (1.0 W/cm^2) [40]. After irradiating the column for only 60 s, its diameter changes from 0.5 to 2.6 mm and length changes from 8 to 2.8 mm, confirming the satisfied *in vivo* activity of the PU/BP implant. These results demonstrate the excellent NIR-photoresponsive shape memory performance of the PU/BP implant, which enable remote control of its shape by the moderate NIR light even being implanted in deep tissue and have large potential to be designed as a contraceptive material.

4. Conclusions

In summary, a new biodegradable NIR-photoresponsive SMP composite has been fabricated based on PU polymer and BP sheets. Under 808 nm light irradiation, the incorporated BP sheets with concentration of only 0.08 wt% enable rapid temperature increase over the T_g of PU and trigger the shape change of the composite with shape recovery rate of ~100%. The *in vitro* and *in vivo* toxicity experiments demonstrate the good biocompatibility of the PU/BP composite, and it degrades naturally into non-toxic carbon dioxide and water from PU and non-toxic phosphate from BP. When implanted into deep tissue with depth of 5 mm in a mice, the PU/BP implant enable the rapid shape change under 808 nm light irradiation with low power intensity of only 0.5 W/cm^2. Together with the excellent NIR-photoresponsive shape memory performance and good biocompatibility with cells and tissues, such biodegradable SMP composite may enable the development of novel “smart” implantable devices for various biomedical applications such as self-expanding stents, active catheters, and controlled drug release, etc.

Acknowledgements

This work was jointly supported by the National Natural Science Fund of China Nos. 51672305, 51602204 and 31771041, Frontier Research Key Project of the Chinese Academy of Sciences No. QYZDB-SSW-SLH034, Shenzhen Science and Technology Research Funding No. JCYJ201602293000503, Leading Talents of Guangdong Province Program No. 00201520, Program of Public Interest Research and Capability Construction of Guangdong Province No. 2015A020217010, Youth Talents of Guangdong Science and Technology Innovation Grant No. 2015TQ01X076, National High-Tech Research and development Program No. 2015AA020316, and Hong Kong Research Grants Council (RGC) General Research Funds (GRF) No. CityU 11301215.

Appendix A. Supplementary data

Supplementary data related to this article can be found at https://doi.org/10.1016/j.biomaterials.2018.02.040.

References

[1] A. Lendlein, S. Kelch, Shape-memory polymers, Angew. Chem. Int. Ed. 41 (2002) 2034–2057.
[2] Q. Zhao, H.J. Qi, T. Xie, Recent progress in shape memory polymer: new behavior, enabling materials, and mechanistic understanding, Prog. Polym. Sci. 49 (2015) 79–120.
[3] A. Lendlein, R. Langer, Biodegradable, elastic shape-memory polymers for potential biomedical applications, Science 296 (2002) 1673–1676.
[4] M.C. Chen, H.W. Tsai, Y. Chang, W.Y. Lai, F.L. Mi, C.T. Liu, et al., Rapidly self-expandable polymeric stents with a shape-memory property, Biomacromolecules 8 (2007) 2774–2780.
[5] L. Xue, S. Dai, Z. Li, Biodegradable shape-memory block co-polymers for fast self-expandable stents, Biomaterials 31 (2010) 8132–8140.
[6] K. Kratz, U. Voigt, A. Lendlein, Temperature-memory effect of copolyesterurethanes and their application potential in minimally invasive medical technologies, Adv. Funct. Mater. 22 (2012) 3057–3065.
[7] T.L. Landsman, T. Touchet, S.M. Hasan, C. Smith, B. Russell, J. Rivera, et al., A shape memory foam composite with enhanced fluid uptake and bactericidal properties as a hemostatic agent, Acta Biomater. 47 (2017) 91–99.
[8] C.S. Yang, H.C. Wu, J.S. Sun, H.M. Hsiao, T.W. Wang, Thermo-induced shape-memory PEG-PCL copolymer as a dual-drug-eluting biodegradable stent, ACS Appl. Mater. Interfaces 5 (2013) 10985–10994.
[9] A. Metcalfe, A.C. Desfaits, I. Salazkin, L.H. Yahia, W.M. Sokolowski, J. Raymond, Cold hibernated elastic memory foams for endovascular interventions, Biomaterials 24 (2003) 491–497.
[10] H. Koerner, G. Price, N.A. Pearce, M. Alexander, R.A. Vaia, Remotely actuated polymer nanocomposites-stress-recovery of carbon-nanotube-filled thermoplastic elastomers, Nat. Mater. 3 (2004) 115–120.
[11] C. Liu, S.B. Chun, P.T. Mather, L. Zheng, E.H. Haley, E.B. Coughlin, Chemically cross-linked polycyclooctene: synthesis, characterization, and shape memory behavior, Macromolecules 35 (2002) 9868–9874.
[12] Y. Zhang, Y. Li, W. Liu, Dipole-dipole and H-bonding interactions significantly enhance the multifaceted mechanical properties of thermoresponsive shape memory hydrogels, Adv. Funct. Mater. 25 (2015) 471–480.
[13] M.Y. Razzaq, M. Anhalt, L. Frormann, B. Weidenfeller, Thermal, electrical and magnetic studies of magnetite filled polyurethane shape memory polymers, Mater. Sci. Eng. 444 (2007) 227–235.
[14] R. Mohr, K. Kratz, T. Weigel, M. Lucka-Gabor, M. Moneke, A. Lendlein, Initiation of shape-memory effect by inductive heating of magnetic nanoparticles in thermoplastic polymers, Proc. Natl. Acad. Sci. U.S.A. 103 (2006) 3540–3545.
[15] D. Habault, H. Zhang, Y. Zhao, Light-triggered self-healing and shape-memory polymers, Chem. Soc. Rev. 42 (2013) 7244–7256.
[16] K.C. Hribar, R.B. Metter, J.L. Ifkovits, T. Troxler, J.A. Burdick, Light-induced temperature transitions in biodegradable polymer and nanorod composites, Small 5 (2009) 1830–1834.
[17] Y. Liu, B. Shaw, M.D. Dickey, J. Genzer, Sequential self-folding of polymer sheets, Sci. Adv 3 (2017) e1602417.
[18] D.H. Yi, H.J. Yoo, S.S. Mahapatra, Y.A. Kim, J.W. Cho, The synergistic effect of the combined thin multi-walled carbon nanotubes and reduced graphene oxides on photothermally actuated shape memory polyurethane, J. Colloid Interface Sci. 432 (2014) 128–134.
[19] T. Xie, Tunable polymer multi-shape memory effect, Nature 464 (2010) 267–270.
[20] H. Xu, C. Yu, S. Wang, V. Malyarchuk, T. Xie, J.A. Rogers, Deformable, programmable, and shape-memorizing micro-optics, Adv. Funct. Mater. 23 (2013) 3299–3306.
[21] M. Burnworth, L. Tang, J.R. Kumpfer, A.J. Duncan, F.L. Beyer, G.L. Fiore, et al., Optically healable supramolecular polymers, Nature 472 (2011) 334–337.
[22] A. Lendlein, H. Jiang, O. Jünger, R. Langer, Light-induced shape-memory polymers, Nature 434 (2005) 879–882.
[23] H. Jiang, S. Kelch, A. Lendlein, Polymers move in response to light, Adv. Mater 18 (2006) 1471–1475.

[24] R. Weissleder, A clearer vision for in vivo imaging, Nat. Biotechnol. 19 (2001), 316–316.
[25] Z. Cheng, T. Wang, X. Li, Y. Zhang, H. Yu, NIR-vis-UV light-responsive actuator films of polymer-dispersed liquid crystal/graphene oxide nanocomposites, ACS Appl. Mater. Interfaces 7 (2015) 27494–27501.
[26] C.H. Zhu, Y. Lu, J. Peng, J.F. Chen, S.H. Yu, Photothermally sensitive poly (N-isopropylacrylamide)/graphene oxide nanocomposite hydrogels as remote light-controlled liquid microvalves, Adv. Funct. Mater. 22 (2012) 4017–4022.
[27] D.J. Maitland, M.F. Metzger, D. Schumann, A. Lee, T.S. Wilson, Photothermal properties of shape memory polymer micro-actuators for treating stroke, Lasers Surg. Med 30 (2002) 1–11.
[28] H. Zhang, H. Xia, Y. Zhao, Optically triggered and spatially controllable shape-memory polymer-gold nanoparticle composite materials, J. Mater. Chem. 22 (2012) 845–849.
[29] Z. Wang, S. Liu, J. Ma, G. Qu, X. Wang, S. Yu, et al., Silver nanoparticles induced RNA polymerase-silver binding and RNA transcription inhibition in erythroid progenitor cells, ACS Nano 7 (2013) 4171–4186.
[30] C. Qua, L. Wang, J. He, J. Tan, W. Liu, S. Zhang, et al., Carbon nanotubes provoke inflammation by inducing the pro-inflammatory genes IL-1β and IL-6, Gene 493 (2012) 9–12.
[31] L. Li, Y. Yu, G.J. Ye, Q. Ge, X. Ou, H. Wu, et al., Black phosphorus field-effect transistors, Nat. Nanotechnol. 9 (2014) 372–377.
[32] F. Xia, H. Wang, Y. Jia, Rediscovering black phosphorus as an anisotropic layered material for optoelectronics and electronics, Nat. Commun. 5 (2014) 4458.
[33] J. Qiao, X. Kong, Z.X. Hu, F. Yang, W. Ji, High-mobility transport anisotropy and linear dichroism in few-layer black phosphorus, Nat. Commun. 5 (2014) 4475.
[34] X. Wang, A.M. Jones, K.L. Seyler, V. Tran, Y. Jia, H. Zhao, et al., Highly anisotropic and robust excitons in monolayer black phosphorus, Nat. Nanotechnol. 10 (2015) 517–521.
[35] X. Zhang, H. Xie, Z. Liu, C. Tan, Z. Luo, H. Li, et al., Black phosphorus quantum dots, Angew. Chem. Int. Ed. 54 (2015) 3653–3657.
[36] C.R. Ryder, J.D. Wood, S.A. Wells, Y. Yang, D. Jariwala, T.J. Marks, et al., Covalent functionalization and passivation of exfoliated black phosphorus via aryl diazonium chemistry, Nat. Chem. 8 (2016) 597–602.
[37] R.A. Doganov, E.C.T. O'Farrell, S.P. Koenig, Y. Yeo, A. Ziletti, A. Carvalho, et al., Transport properties of pristine few-layer black phosphorus by van der waals passivation in an inert atmosphere, Nat. Commun. 6 (2015) 6647.
[38] S. Lin, S. Liu, Z. Yang, Y. Li, T.W. Ng, Z. Xu, Solution-processable ultrathin black phosphorus as an effective electron transport layer in organic photovoltaics, Adv. Funct. Mater. 26 (2016) 864–871.
[39] Z. Sun, H. Xie, S. Tang, X.F. Yu, Z. Guo, J. Shao, et al., Ultrasmall black phosphorus quantum dots: synthesis and use as photothermal agents, Angew. Chem. 127 (2015) 11688–11692.
[40] J. Shao, H. Xie, H. Huang, Z. Li, Z. Sun, Y. Xu, et al., Biodegradable black phosphorus-based nanospheres for in vivo photothermal cancer therapy, Nat. Commun. 7 (2016) 12967.
[41] Z. Sun, Y. Zhao, Z. Li, H. Cui, Y. Zhou, W. Li, et al., TiL_4-coordinated black phosphorus quantum dots as an efficient contrast agent for in vivo photoacoustic imaging of cancer, Small 13 (2017), https://doi.org/10.1002/smll.201602896.
[42] C. Sun, L. Wen, J. Zeng, Y. Wang, Q. Sun, L. Deng, et al., One-pot solventless preparation of PEGylated black phosphorus nanoparticles for photoacoustic imaging and photothermal therapy of cancer, Biomaterials 91 (2016) 81–89.
[43] H. Wang, X. Yang, W. Shao, S. Chen, J. Xie, X. Zhang, et al., Ultrathin black phosphorus nanosheets for efficient singlet oxygen generation, J. Am. Chem. Soc. 137 (2015) 11376–11382.
[44] W. Tao, X. Zhu, X. Yu, X. Zeng, Q. Xiao, X. Zhang, et al., Black phosphorus nanosheets as a robust delivery platform for cancer theranostics, Adv. Mater. 29 (2017) 1603276.
[45] W. Chen, J. Ouyang, H. Liu, M. Chen, K. Zeng, J. Sheng, et al., Black phosphorus nanosheet-based drug delivery system for synergistic photodynamic/photothermal/chemotherapy of cancer, Adv. Mater 29 (2016) 1603864.
[46] H.U. Lee, S.Y. Park, S.C. Lee, S. Choi, S. Seo, H. Kim, et al., Black phosphorus (BP) nanodots for potential biomedical applications, Small 12 (2016) 214–219.
[47] J. Kang, J.D. Wood, S.A. Wells, J.H. Lee, X. Liu, K.S. Chen, et al., Solvent exfoliation of electronic-grade, two-dimensional black phosphorus, ACS Nano 9 (2015) 3596–3604.
[48] P. Yasaei, B. Kumar, T. Foroozan, C. Wang, M. Asadi, D. Tuschel, et al., High-quality black phosphorus atomic layers by liquid-phase exfoliation, Adv. Mater 27 (2015) 1887–1892.
[49] Z. Guo, H. Zhang, S. Lu, Z. Wang, S. Tang, J. Shao, et al., From black phosphorus to phosphorene: basic solvent exfoliation, evolution of Raman scattering, and applications to ultrafast photonics, Adv. Funct. Mater. 25 (2015) 6996–7002.
[50] Y. Huang, J. Qiao, K. He, S. Bliznakov, E. Sutter, X. Chen, et al., Degradation of Black Phosphorus (BP): the Role of Oxygen and Water, 2015 arXiv preprint arXiv:1511.09201.
[51] X. Ling, H. Wang, S. Huang, F. Xia, M.S. Dresselhaus, The renaissance of black phosphorus, Proc. Natl. Acad. Sci. U.S.A. 112 (2015) 4523–4530.
[52] C. Ruan, Y. Wang, M. Zhang, Y. Luo, C. Fu, M. Huang, et al., Design, synthesis and characterization of novel biodegradable shape memory polymers based on poly (D, L-lactic acid) diol, hexamethylene diisocyanate and piperazine, Polym. Int. 61 (2012) 524–530.
[53] C. Ruan, N. Hu, Y. Hu, L. Jiang, Q. Cai, H. Wang, et al., Piperazine-based polyurethane-ureas with controllable degradation as potential bone scaffolds, Polymer 55 (2014) 1020–1027.
[54] J. Abranches, M.M. Nascimento, L. Zeng, C.M. Browngardt, Z.T. Wen, M.F. Rivera, et al., CcpA regulates central metabolism and virulence gene expression in streptococcus mutans, J. Bacteriol. 190 (2008) 2340–2349.
[55] Y. Wang, G. Huang, H. Mu, S. Lin, J. Chen, S. Xiao, et al., Ultrafast recovery time and broadband saturable absorption properties of black phosphorus suspension, Appl. Phys. Lett. 107 (2015) 091905.
[56] H. Xie, Z. Li, Z. Sun, J. Shao, X.F. Yu, Z. Guo, et al., Metabolizable ultrathin Bi_2Se_3 nanosheets in imaging-guided photothermal therapy, Small 12 (2016) 4136–4145.
[57] T. Liu, S. Shi, C. Liang, S. Shen, L. Cheng, C. Wang, et al., Iron oxide decorated MoS_2 nanosheets with double PEGylation for chelator-free radiolabeling and multimodal imaging guided photothermal therapy, ACS Nano 9 (2015) 950–960.
[58] X. Yang, M. Yang, B. Pang, M. Vara, Y. Xia, Gold nanomaterials at work in biomedicine, Chem. Rev. 115 (2015) 10410–10488.
[59] J.T. Robinson, S.M. Tabakman, Y. Liang, H. Wang, H.S. Casalongue, D. Vinh, et al., Ultrasmall reduced graphene oxide with high near-infrared absorbance for photothermal therapy, J. Am. Chem. Soc. 133 (2011) 6825–6831.
[60] L. Cheng, J.J. Liu, X. Gu, H. Gong, X.Z. Shi, T. Liu, et al., PEGylated WS_2 nanosheets as a multifunctional theranostic agent for in vivo dual-modal CT/photoacoustic imaging guided photothermal therapy, Adv. Mater 26 (2014) 1886–1893.
[61] R. Luo, J. Wu, N.D. Dinh, C.H. Chen, Gradient porous elastic hydrogels with shape-memory property and anisotropic responses for programmable locomotion, Adv. Funct. Mater. 25 (2015) 7272–7279.
[62] Q. Shou, K. Uto, W.C. Lin, T. Aoyagi, M. Ebara, Near-infrared-irradiation-induced remote activation of surface shape-memory to direct cell orientations, Macromol. Chem. Phys. 215 (2014) 2473–2481.
[63] K. Kornicka, K. Marycz, K.A. Tomaszewski, M. Marędziak, A. Śmieszek, The effect of age on osteogenic and adipogenic differentiation potential of human adipose derived stromal stem cells (hASCs) and the impact of stress factors in the course of the differentiation process, Oxid. Med. Cell. Longevity 2015 (2015) 309169.
[64] Y. Wang, C. Ruan, J. Sun, M. Zhang, Y. Wu, K. Peng, Degradation studies on segmented polyurethanes prepared with poly (D, L-lactic acid) diol, hexamethylene diisocyanate and different chain extenders, Polym. Degrad. Stab 95 (2011) 1687–1694.
[65] X.D. Zhang, J. Chen, Y. Min, G.B. Park, X. Shen, S.S. Song, et al., Metabolizable Bi_2Se_3 nanoplates: biodistribution, toxicity, and uses for cancer radiation therapy and imaging, Adv. Funct. Mater. 24 (2014) 1718–1729.
[66] S. Tang, C.Y. Zhang, M.N. Huang, Y.F. Luo, Z.Q. Liang, Fallopian tube occlusion with a shape memory polymer device: evaluation in a rabbit model, Contraception 87 (2013) 235–241.